Title

Energy Decomposition Analysis for Excimers Using Absolutely Localized Molecular Orbitals within Time-Dependent Density Functional Theory and Configuration Interaction with Single Excitations.

Journal

Journal of chemical theory and computation, 14(10)

ISSN

1549-9618

Authors

Ge, Qinghui

Head-Gordon, Martin

Publication Date

2018-10-01

DOI

10.1021/acs.jctc.8b00537

Peer reviewed

Energy decomposition analysis for excimers using absolutely localized molecular orbitals within time-dependent density functional theory and configuration interaction with single excitations

Qinghui Ge[†,‡] and Martin Head-Gordon[*,†,‡]

† *Kenneth S. Pitzer Center for Theoretical Chemistry, Department of Chemistry, University of California at Berkeley, Berkeley, CA 94720, USA*

‡ *Chemical Science Division, Lawrence Berkeley National Laboratory, Berkeley, CA 94720, USA*

E-mail: mhg@cchem.berkeley.edu

Abstract

We present an improved energy decomposition analysis (EDA) scheme for understanding intermolecular interactions in delocalized excited states, especially in excimers. In the EDA procedure, excited states are treated with linear response theory such as configuration interaction singles (CIS) or time-dependent density functional theory (TDDFT), and absolutely localized molecular orbitals (ALMOs) are used to define the intermediate (frozen, excitonic coupling, and polarized) states. The intermolecular interaction energy is thereby separated into frozen, excitonic splitting, polarization and charge transfer contributions. The excitonic splitting term describes

the delocalization effect as two or more degenerate local excitations couple with each other, which is often an important binding force in excimers. A maximum overlap state-tracking procedure is introduced to connect the initial fragment excitations to the constrained intermediate states, and finally to the unconstrained delocalized states of the complex. The EDA scheme is applied to several excimer systems, including the He_2^* and Ne_2^* noble gas excimers, the doubly hydrogen-bonded 2-pyridone dimer, and the aromatic benzene and perylene excimers. We are able to gain some useful insights into the role each term is playing in the formation of these excimers, and the resulting method may also be useful for understanding a range of other complexes in excited states.

1 Introduction

Excimers are excited dimers that, while weakly bound in the ground state, are much more strongly interacting in the electronic excited state. In fluorescence spectra, excimer emission typically appears as a broad, structureless band at lower energy than the structured molecular band. One well-known example of excimers occurs in the noble gas dimers.[1] He_2^* was the first singlet excimer to be identified though fluorescence spectra.[2] It can be thought of as a He_2^+ core (with bond order 1/2), and an outer Rydberg electron. An intense continuum between 60 nm and 100 nm was attributed to the transition from He_2^* to the dissociated ground state (He + He). Other noble gases excimers (Ne_2^*, Ar_2^*, Kr_2^*) were subsequently discovered.[3–5] Aromatic molecules can also form excimers in solution, as well as in neat liquid, molecular crystals and polymers.[1] The most stable excimer structure is usually perfectly stacked, consisting of a symmetric pair of parallel molecules. The pyrene dimer was the first experimentally studied aromatic system,[6] and its fluorescence quenching has been used as an effective analytical tool.[7–11]

There are two main types of configuration interaction (CI) which can contribute to excimer formation: (1) exciton resonance (ER) caused by interaction between localized excited states ($A^*B \leftrightarrow AB^*$), where the electron and hole are placed on the same molecule. (2) charge resonance (CR) due to interaction between charge transfer states ($A^+B^- \leftrightarrow A^-B^+$). The excimer states originate from a mixture of ER and CR states, and simplified models of excimer formation based only on ER or CR may not properly explain some experimental results.[1] The Frenkel-Davydov exciton model,[12,13] for example, only gives rise to pure ER states as its wavefunction is constructed in the basis of neutral excitations:

$$|\Phi\rangle = c_A|\Psi_A^*\Psi_B\rangle + c_B|\Psi_A\Psi_B^*\rangle \tag{1}$$

and the coefficient c_A and c_B are solved from the corresponding secular equation. The off-

diagonal term $\langle \Psi_A^* \Psi_B | \hat{H} | \Psi_A \Psi_B^* \rangle$, coming from the coupling between localized excitations, are sometimes estimated as Coulomb integrals over transition densities[14] or simply within a dipole approximation. This will tend to be inaccurate at short separations. *Ab initio* implementation of the Frenkel exciton model, which takes account of exact exchange and the overlap between localized states was recently proposed by Herbert and coworkers.[15] In order to study systems where charge-transfer (CT) plays an important role, efforts have been made to go beyond the Frenkel exciton model, often by expanding the basis space for CI to include charge-transfer basis states.[16,17]

The formation of excimers can also be viewed from the perspective of intermolecular interactions. Energy decomposition analysis (EDA) is a powerful tool to study intermolecular interactions.[18,19] An EDA decomposes the total interaction energy into several interpretable components, such as electrostatics, Pauli repulsion, dispersion, polarization and charge transfer, thereby allowing an assessment of their relative importance. Many EDA schemes have been proposed and used for studying intermolecular interactions between ground state molecules,[20–44] and we believe that a suitably designed EDA can also help in understanding the relative roles of the different driving forces that given rise to excimers. For example, it would be very useful to distinguish the comparative magnitude of the ER and CR effects mentioned above. It should be mentioned that many wavefunction analysis schemes have been proposed to quantify the ER and/or CR characters of excited states using quantities related to the transition or difference density matrix.[45–51] Nonetheless, these "top-down" analysis schemes focus more on the composition and general character of an excited state wavefunction rather than the energy components that lead to the formation of an excimer. In broader terms, there is far greater chemical understanding of intermolecular interactions in the ground state of complexes than those in excited states, and therefore a well-posed EDA for excited states can be even more valuable than one for ground states. One reason for this is that monomer properties such as polarizabilities and Lewis acidity or

basicity can be drastically different in excited states, and another reason is that the exciton resonance effect is unfamiliar from ground states.

There are very few reported EDA approaches for unraveling the electronic structure of complexes in excited states. Recently, we proposed an EDA scheme for understanding intermolecular interactions involving excited molecules.[52] This EDA was formulated in the framework of linear response theory for single excitations (e.g. configuration interaction singles (CIS)[53,54] and time-dependent density functional theory (TDDFT)[53,55–57] within the Tamm-Dancoff approximation (TDA)[58]) and utilized absolutely localized molecular orbitals (ALMOs)[59,60] to define the intermediate (frozen and polarized) states. The formulation of that method assumes that one of the fragments has an excitation energy considerably lower than the other fragments, so the excitation can be assigned to a single molecule within a complex (i.e. exciplexes). This assumption is appropriate for cases such as solvated chromophores, but not for excimer systems.

In this work, we take up the challenge of generalizing the previously proposed EDA scheme for exciplexes to treat excimers. Briefly speaking, in the exciplex EDA, the shift in excitation energy when an excited molecule interacts with the environment was separated into three terms: frozen (FRZ), polarization(POL) and charge transfer(CT), and each term was then added to its counterparts obtained from the original ground state ALMO-EDA.[36,40] Here, we will introduce a new term which we call excitonic-splitting (EXSP) to account for the coupling between local excitations (i.e. the ER effect). Details of the excimer EDA formulation are presented in Sec. 2. In Sec. 3, we apply the new EDA scheme to several representative examples, including the noble gas and aromatic excimers.

2 Theory

The new EDA scheme employed in this paper is closely related to the ALMO-EDA for exciplexes that we proposed recently.[52] The two schemes share the same definition for the frozen and polarized states. Therefore, we will first review our previous scheme but carefully write down the derivation for multiple states, as at least two states are considered in excimer systems. Then we introduce the excitonic splitting term and the excitonic coupling intermediate state, which are important for excimers. Finally we propose a state tracking approach that is essential for connecting the initial fragment-localized states to the final delocalized excited states of the complex.

In this section and the rest of this paper, molecular orbitals are denoted by lowercase letters i, j (occupied) and a, b (virtual). Capital letters I, J are used as subscript indicate fragments indexes. The state indexes are denoted in the superscript: s, t for fragment states, κ, κ' for supersystem states, "$*$" for a generic excited state and superscripts are often dropped in the case of a ground state. In Sec. 3, we also use symbols for irreducible representations to specify excited states based on the symmetry of molecular wavefunctions.

2.1 Review of ALMO-EDA for exciplexes

By definition, the interaction energy is the counterpoise (CP)-corrected[61] difference between the excited supersystem energy E^* and the sum of isolated fragment energies, E^*_{frag}:

$$\Delta E^*_{\text{INT}} = E^* - E^*_{\text{frag}} + \Delta E_{\text{BSSE}} \tag{2}$$

where the last term represents the basis set superposition error (BSSE). When the excitation of interest is mainly localized on one fragment (assuming it is fragment 1 without loss of generality), E^*_{frag} is defined as the sum of excited state energy of fragment 1 and ground state

energies of other fragments. Equivalently, this is equal to the sum of ground state energies for all fragments and ω_1, the excitation energy of fragment 1 in isolation.

$$E^*_{\rm frag} = E^*_1 + \sum_{J>1}^{N} E_J = \sum_{J=1}^{N} E_J + \omega_1 \tag{3}$$

Let us turn to systems composed of identical fragments. Assume there are M excitations of the isolated fragments that are close in energy. This will typically be one excitation per fragment if the fragments are identical, but can in principle involve more than one excited state per fragment. We can now define M different $E_{\rm frag}$'s, each one corresponding to a particular excitation from the M degenerate excitations. For example, the κ^{th} reference energy, which corresponds to excited state s of fragment I is:

$$E^\kappa_{\rm frag} = E^s_I + \sum_{J\neq I}^{N} E_J = \sum_{J}^{N} E_J + \omega^s_I$$

The M fragment excitations are likely to mix when the fragments interact, and form M supersystem excited states that are delocalized across fragments. Let us label these state energies as E^κ. While the local excitations are degenerate or near-degenerate, the supersystem states will usually split due to interaction, resulting in a range of different E^κ values.

To understand the effect of interaction, one needs to look at a set of M interaction energies, one for each resulting state: $\Delta E^\kappa_{\rm INT} = E^\kappa - E^\kappa_{\rm frag} + \Delta E^\kappa_{\rm BSSE}$. For each such interaction energy, $\Delta E^\kappa_{\rm INT}$, the contribution from the ground state interaction energy, $\Delta E_{\rm INT}$ and the shift in excitation energy, $\Delta\omega_{\rm INT}$, can be separated:

$$\Delta E^\kappa_{\rm INT} = \Delta E_{\rm INT} + \Delta\omega^\kappa_{\rm INT} \tag{4}$$

where $\Delta E_{\rm INT} = E - \sum_{I=1}^{N} E_I$, $\Delta\omega^\kappa_{\rm INT} = \omega^\kappa - \omega^s_I$. Our exciplex EDA scheme[52] decomposes the excited cluster interaction energy into three terms, frozen (FRZ), polarization (POL) and

charge transfer (CT). This is achieved by first defining the frozen and polarized wavefunction of excited states. Now, with the degeneracy between fragments present, we need to consider M frozen and polarization intermediate states, each defined in a similar way as before.

Polarized excited systems are described by the ALMO-CIS[62] wavefunction (or its TDDFT or TDDFT/TDA analog as appropriate), and $E^{\kappa}_{\mathrm{POL}}$ is given by the ALMO-CIS energy of state κ. The difference between $E^{\kappa}_{\mathrm{POL}}$ and E^{κ} results from the constraint in ALMO-CIS that the excitation can only take place between an occupied and a virtual orbital on the same fragment, and the ALMOs only contain contributions from the atomic orbital (AO) basis functions that reside on the given fragment. With these constraints, the ALMO-CIS states are intuitively CT-free (see the Appendix of ref. 63 for a proof). Thus the CT terms can be defined as:

$$\Delta E^{\kappa}_{\mathrm{CT}} = E^{\kappa} - E^{\kappa}_{\mathrm{POL}} + \Delta E^{\kappa}_{\mathrm{BSSE}} \tag{5}$$

Recalling that in the ground state ALMO-EDA, SCF(MI) is used to compute the polarized system energy E_{POL}, the CT term can also be rewritten as:

$$\begin{aligned} \Delta E^{\kappa}_{\mathrm{CT}} &= (E - E_{\mathrm{POL}} + \Delta E_{\mathrm{BSSE}}) \\ &\quad + (\omega^{\kappa} - \omega^{\kappa}_{\mathrm{POL}} + \Delta E^{\kappa}_{\mathrm{BSSE}} - \Delta E_{\mathrm{BSSE}}) \\ &= \Delta E_{\mathrm{CT}} + \Delta \omega^{\kappa}_{\mathrm{CT}} \end{aligned} \tag{6}$$

In the frozen wavefunction, both amplitudes and orbitals are frozen. We compute the

κ^{th} frozen excitation energy using the singles amplitudes of the isolated fragment, $t^\kappa \equiv t_I^s$:

$$\begin{aligned}\omega_{\mathrm{FRZ}}^\kappa = & \sum_{i,a,j,b\in I} (F_{ab}S_{ij}t_I^{s,ia}t_I^{s,jb} - F_{ij}S_{ab}t_I^{s,ia}t_I^{s,jb}) \\ & + \sum_{i,a,j,b\in I} \langle\psi_i\psi_b||\psi_a\psi_j\rangle t_I^{s,ia}t_I^{s,jb} \\ & + 2\sum_{i,a\in I} F_{ia}z_I^{s,ia} \end{aligned} \tag{7}$$

where **F** and **S** are the Fock and overlap matrices in the MO basis, respectively, and ψ's represent the MOs. The necessity of including the occupied-virtual block of the relaxed density of the isolated fragment (z_I) is discussed by Thirman *et al.* in the development of MP2-ALMO-EDA,[41] as well as in our previous EDA scheme for exciplexes.[52] The frozen contribution to the excitation energies and the excited system energies are:

$$\begin{aligned}\Delta\omega_{\mathrm{FRZ}}^\kappa &= \omega_{\mathrm{FRZ}}^\kappa - \omega_I^s \\ \Delta E_{\mathrm{FRZ}}^\kappa &= \Delta E_{\mathrm{FRZ}} + \Delta\omega_{\mathrm{FRZ}}^\kappa \end{aligned} \tag{8}$$

Further decomposition of the frozen energy is also possible in ground state EDA.[64] A simple scheme (e.g. see ref. 65) is to use the "quasi-classical" definition for permanent electrostatics,

and to classify the remainder of the frozen energy as Pauli repulsion:

$$\Delta E^{\kappa}_{\mathrm{ELEC}} = \sum_{K<L} \int \int \mathrm{d}\mathbf{r}_1 \mathrm{d}\mathbf{r}_2 \rho^{\mathrm{tot}}_K(\mathbf{r}_1) r^{-1}_{12} \rho^{\mathrm{tot}}_L(\mathbf{r}_2)$$

with

$$\rho^{\mathrm{tot}}_K = \begin{cases} \rho^s_I(\mathbf{r}) + \rho^{\mathrm{nuc}}_I(\mathbf{r}) & K = I \\ \rho_K(\mathbf{r}) + \rho^{\mathrm{nuc}}_K(\mathbf{r}) & K \neq I \end{cases} \tag{9}$$

and

$$\Delta E^{\kappa}_{\mathrm{PAULI}} = \Delta E^{\kappa}_{\mathrm{FRZ}} - \Delta E^{\kappa}_{\mathrm{ELEC}} \tag{10}$$

where ρ represents the ground state fragment electronic density, ρ^s_I is the s^{th} excited state electronic density of fragment I, and ρ^{nuc} and ρ^{tot} are the nuclear and total fragment charge densities, respectively. Defined in this way, the Pauli term will inevitably be contaminated by dispersion if the employed model chemistry incorporates long-range correlation effects (e.g. van der Waals density functionals).

2.2 Introducing the excitonic splitting term

Up to this point, the derivation largely follows the previous EDA scheme, except that the terms are now defined explicitly for each state. We will now introduce the main generalization needed in order to study the role of excitonic couplings, as are expected to be prevalent in systems with degenerate monomer excited states. Previously, any interaction energy difference between the frozen and polarized intermediate states was attributed to polarization effects. Now, as more than one fragment may make a significant contribution to the supersystem excitation, any coupling between these local excitations may break the degeneracy of the isolated monomer excitations. For identical fragments (and identical environment for each fragment), the frozen states are also degenerate, and the splitting due to configuration

interaction between degenerate states will occur as soon as it is allowed (i.e. at the polarized level).

To separate the splitting effect due to "pure excitonic coupling" (i.e. the mixing of degenerate configurations) from polarization (i.e. changes in the on-fragment charge distributions due to the electrostatic environment), we propose a new EDA term, $\Delta\omega_{\mathrm{EXSP}}$, whose associated intermediate state has the form of a linear combination of the (degenerate) local excitations:

$$|\Phi_{\mathrm{EXSP}}\rangle = \sum_{\kappa}^{M} c^{\kappa} |\Psi_1 \Psi_2 ... \Psi_I^s ... \Psi_N\rangle \tag{11}$$

The coefficients $c^{\kappa} \equiv c_I^s$ and the corresponding excitonic-splitting excitation energies ω_{EXSP} are determined by solving the Schrödinger equation in the basis of the local excitations:

$$\mathcal{A}c = \omega_{\mathrm{EXSP}} \mathcal{G} c \tag{12}$$

The Hamiltonian $\mathcal{A}$ and metric $\mathcal{G}$ have dimension $M \times M$, with M being the total number of degenerate local excitations considered. This excitonic term is to be evaluated *before* the polarized intermediate state is considered.

The matrix elements are computed as:

$$\begin{aligned}
\mathcal{A}_{\kappa\kappa'} &= \langle \Psi_{\kappa} | \hat{H} - E_{\mathrm{FRZ}} | \Psi_{\kappa'} \rangle + \text{response} \\
&= \sum_{i,a\in I,j,b\in J} (F_{ab} S_{ij} t_I^{s,ia} t_J^{r,jb} - F_{ij} S_{ab} t_I^{s,ia} t_J^{r,jb}) \\
&+ \sum_{i,a\in I,j,b\in J} \langle \psi_i \psi_b || \psi_a \psi_j \rangle t_I^{s,ia} t_J^{r,jb} \\
&+ \sum_{i,a\in I} F_{ia} z_I^{s,ia} \delta_{\kappa\kappa'} \\
\mathcal{G}_{\kappa\kappa'} &= \langle \Psi_{\kappa} | \Psi_{\kappa'} \rangle \\
&= \sum_{i,a\in I,j,b\in J} S_{ij} S_{ab} t_I^{s,ia} t_J^{r,jb}
\end{aligned}$$

Here, in general, index κ corresponds to state s on fragment I, and κ' corresponds to state r on fragment J. In the simple case of one degenerate state per fragment, κ reduces to simply be a fragment index. Note that the occupied orbitals are projected out of the virtual space, and the virtual orbitals are reorthogonalized within each fragment (as in Eq. 7). The response terms are added to the diagonal to ensure that the diagonal elements are the same as in Eq. 7. For simplicity, the off-diagonal elements are unmodified. Apart from simplicity, a further argument for this choice is $z_{IJ} = 0$, as the RHS of the z vector equation is in fact the response of energy to orbital rotations, and interfragment orbital rotation is forbidden at the frozen level. In this way, the new model is consistent with the previous one, since if the energy gap between different local excitations is large (compared to the magnitude of coupling), the eigenvalues of Eq. 12 are just the diagonal elements, i.e., the frozen energies. The other extreme is that all local excitations are degenerate.

In the simplest case of two identical fragments each contributing one state, we have a 2×2 generalized eigenvalue problem:

$$\begin{pmatrix} \omega_{\mathrm{FRZ}} & V \\ V & \omega_{\mathrm{FRZ}} \end{pmatrix} \begin{pmatrix} c_1 \\ c_2 \end{pmatrix} = \omega_{\mathrm{EXSP}} \begin{pmatrix} 1 & S \\ S & 1 \end{pmatrix} \begin{pmatrix} c_1 \\ c_2 \end{pmatrix}$$

where V and S are the off-diagonal elements of the Hamiltonian $\mathcal{A}$ and the metric $\mathcal{G}$, respectively. The solution to this 2×2 problem is

$$\begin{aligned} |\Phi^{-}_{\mathrm{EXSP}}\rangle &= (|\Psi_1^* \Psi_2\rangle - |\Psi_1 \Psi_2^*\rangle)/\sqrt{2(1-S)} \\ \omega^{-}_{\mathrm{EXSP}} &= \frac{(1+S)(\omega_{\mathrm{FRZ}} - V)}{1-S} \\ |\Phi^{+}_{\mathrm{EXSP}}\rangle &= (|\Psi_1^* \Psi_2\rangle + |\Psi_1 \Psi_2^*\rangle)/\sqrt{2(1+S)} \\ \omega^{+}_{\mathrm{EXSP}} &= \frac{(1-S)(\omega_{\mathrm{FRZ}} + V)}{1+S} \end{aligned} \tag{13}$$

One can see that the two resulting states are fully delocalized, with the one state having lower excitation energy compared to the localized frozen states, the other state has an increased excitation energy. This shares the same spirit as the Frenkel exciton model.

ω_{EXSP}'s are the excitation energies taking the excitonic coupling effect into account, but are free of polarization and charge transfer. Therefore, we can define the excitonic splitting terms as the shift from excitation energies at the frozen level:

$$\Delta\omega^{\kappa}_{\mathrm{EXSP}} = \omega^{\kappa}_{\mathrm{EXSP}} - \omega^{\kappa}_{\mathrm{FRZ}} \tag{14}$$

Subsequently the polarization term can then be evaluated via ALMO-CIS/ALMO-TDDFT as

$$\begin{aligned}
\Delta\omega^{\kappa}_{\mathrm{POL}} &= \omega^{\kappa}_{\mathrm{POL}} - \omega^{\kappa}_{\mathrm{EXSP}} \\
\Delta E^{\kappa}_{\mathrm{POL}} &= E^{\kappa}_{\mathrm{POL}} - E^{\kappa}_{\mathrm{EXSP}} \\
&= (E_{\mathrm{POL}} + \omega^{\kappa}_{\mathrm{POL}}) - (E_{\mathrm{FRZ}} + \omega^{\kappa}_{\mathrm{EXSP}}) \\
&= \Delta E_{\mathrm{POL}} + \Delta\omega^{\kappa}_{\mathrm{POL}}
\end{aligned} \tag{15}$$

To summarize, the new EDA scheme requires computing five different energies that correspond to progressively weaker constraints: (1) isolated fragment energies ($E^{\kappa}_{\mathrm{frag}}$); (2) the frozen energy ($E^{\kappa}_{\mathrm{FRZ}}$), which is the energy of the supersystem subject to the constraint that the fragments keep their orbitals and amplitudes unchanged; (3) the excitonic-splitting energy ($E^{\kappa}_{\mathrm{EXSP}}$), which takes the coupling between frozen fragment excited states into account; (4) the energy of polarized states ($E^{\kappa}_{\mathrm{POL}}$) evaluated with ALMO-CIS/ALMO-TDDFT; (5) the full system energy (E^{κ}) evaluated without any constraint. Every time we move to the next level (i.e. to a weaker constraint) the resulting energy change is designated as an EDA term. Among the four EDA terms, the excitonic-splitting term is unique to excited

states (in other words, for the ground state $E_{\mathrm{EXSP}} = 0$). The other three terms (FRZ, POL and CT) all involve a contribution from the ground state (ΔE, obtained from the ground state ALMO-EDA) as well as a correction arising from the excitation energies ($\Delta\omega^{\kappa}$) that is state-specific.

2.3 State-tracking in EDA

Extra caution should be taken when multiple states are involved in EDA. Previously, for systems whose excitations are significantly different, we only focused on the lowest states, which are mainly localized on one fragment and minimally mixed with states on other fragments. Now as the EDA is performed for M excited states, the situation becomes more complicated. There is a straightforward one-to-one mapping only between the isolated fragment states and the frozen states. Defining this mapping is potentially problematic at EDA levels where states are delocalized (EXSP, POL, CT). One cannot simply track state indexes, or even look at just the lowest M states if, say, there is a low-lying charge-resonance state, or the M states switch order since the interactions may affect different states unequally. To make the EDA usable in these interesting and complex settings, we require that the final states maintain the character of the reference isolated fragment states. In other words, it is desirable to be able to view the interfragment interaction as akin to a perturbation, even though we are now allowing a degenerate perturbation theory description.

The problem is addressed by finding the states that most resemble the reference, where the resemblance is measured by the overlaps between states. For example, if Φ_{κ} is the κ state at one intermediate level, and $\tilde{\Phi}_{\kappa'}$ is the κ' state at another level, the overlap between

them is computed as:

$$\begin{aligned} G_{\kappa\kappa'} &= \langle \Phi^{\kappa} | \tilde{\Phi}^{\kappa'} \rangle \\ &= \sum_{ia} \sum_{i'a'} t_{\kappa}^{ia} S_{ii'} S_{aa'} \tilde{t}_{\kappa'}^{i'a'} \end{aligned} \tag{16}$$

Here t and $\tilde{t}$ are amplitudes of Φ_{κ} and $\tilde{\Phi}_{\kappa'}$, respectively, $S_{ii'}$ and $S_{aa'}$ are the MO overlaps, which appear because the frozen, polarized and final wavefunctions use different MOs.

The magnitude of $G_{\kappa\kappa'}$ is between 0 and 1. If $G = |G_{\kappa\kappa'}|$ is close to 1, it means that the two states are very similar. We can keep track of the M states based on the G values: at each intermediate level (including the final), we look for the states that have maximum overlap with states at the previous level, and the EDA terms should take the differences between the pairs of states that overlap the most.

Considering a hypothetical 2×2 case as an example, based on the analysis mentioned above, $G_{11}(\text{FRZ}|\text{EXSP}) \approx G_{22}(\text{FRZ}|\text{EXSP}) \approx 0.5$, as the two local excitations have equal contributions to the EXSP states. After polarization, one may find that $G_{11}(\text{EXSP}|\text{POL}) \approx G_{22}(\text{EXSP}|\text{POL}) \approx 0.99$ while the other overlaps are close to 0. This indicates that the two lowest polarized states are closely related to the EXSP states, and thus the polarization terms would be $\Delta E^1_{\text{POL}} = E^1_{\text{POL}} - E^1_{\text{ESXP}}$, $\Delta E^2_{\text{POL}} = E^2_{\text{POL}} - E^2_{\text{ESXP}}$. Next, with CT included, assume that $G_{11}(\text{POL}|\text{FINAL}) \approx 0.95$, $G_{23}(\text{POL}|\text{FINAL}) \approx 0.80$, and that overlaps between other final states and the two lowest POL states are insignificant. One can then define $\Delta E^1_{\text{CT}} = E^1 - E^1_{\text{POL}} + \Delta E^1_{\text{BSSE}}$, $\Delta E^2_{\text{CT}} = E^3 - E^2_{\text{POL}} + \Delta E^2_{\text{BSSE}}$. The G values also hint at the relative importance of each EDA term. For example, in the above case, CT is likely to have more influence than POL. Note that in these analyses, at most M final states can eventually be mapped into the original fragment states, and these are the exciton resonance states. For states with strong CT character (e.g. the final state 2 above), one may consider utilizing $F1^+F2^-/F1^-F2^+$ instead of $F1^*F2/F1F2^*$ as reference states. However, we will

not examine these charge resonance states any further in this work.

Before moving on, we refer the reader to the Table of Contents (TOC) figure for a schematic illustration of the overall scheme associated with this EDA, where we illustrated how excited states at five distinct stages of constraint (initial, frozen, excitonic-splitting, polarized, and final) are related to each other as well as the possible effects of state crossing.

3 Application Examples

The generalized excited state ALMO-EDA has been implemented in a development version of the Q-Chem electronic structure program.[66] As tests of the new EDA scheme, we apply it to five systems: He_2^*, Ne_2^*, 2-pyridone dimer, benzene excimer and perylene excimer. For all TDDFT calculations, the Tamm-Dancoff approximation (TDA) is employed. All EDA results are CP-corrected, which slightly affects the CT term and the total interaction. For example, for the perylene excimer at the equilibrium structure of the lowest excited (B_{3g}) state, the BSSE estimated by subtracting the CP-corrected and uncorrected interaction energy is 0.125 eV, amounting to roughly 9% of the CP-corrected interaction energy for that state. The basis sets employed for other excimers are larger and therefore the magnitude of the BSSE is smaller in the other cases (see Table S1 of the Supporting Information).

3.1 Noble gas excimer: He_2^* and Ne_2^*

To explore how the new EDA scheme works, we first apply it to He_2^* and Ne_2^*, at an interatomic distance of 3.0 Å (close to the ground state equilibrium geometry). The calculation is performed with CIS (since it is self-interaction-free and these are Rydberg excitations) and a customized 6-311(2+)G basis, which includes two additional sets of diffuse functions to enable a better description of the Rydberg states. Fig. 1 shows the energy levels of these two systems.

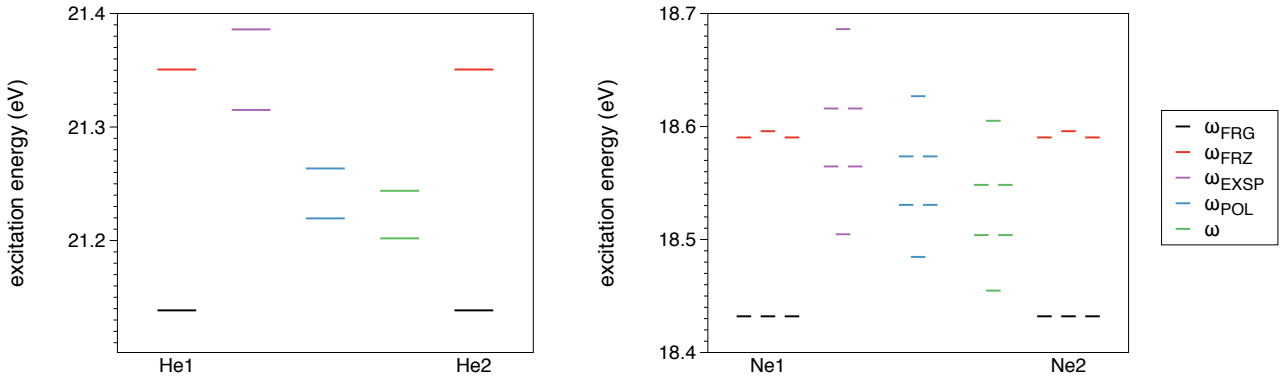

(a) He_2^* (b) Ne_2^*

Figure 1: Excitation energies at different EDA levels for (a) He_2^* and (b) Ne_2^*, The interatomic distance is chosen to be 3.0 Å for both cases. The two states for He_2^* correspond to $1s \rightarrow 2s$ monomer excitations. The six states for Ne_2^* are derived from the $2p_x \rightarrow 3s$, $2p_y \rightarrow 3s$ and $2p_z \rightarrow 3s$ monomer excitations.

For He_2^*, we consider the two lowest singlet excited states (2^1A_{1g}, $^1A_{1u}$) that originate from the $1s \rightarrow 2s$ monomer state. The frozen states remain degenerate, but their excitation energies are 0.212 eV higher than the isolated monomer states. This can be explained by the fact that Pauli repulsion is more unfavorable for the excited states as the electronic density becomes more diffuse upon excitation ($\Delta E_{\mathrm{PAULI}} = 0.001$ eV, $\Delta E^{1,2}_{\mathrm{PAULI}} = 0.269$ eV, $\Delta\omega^{1,2}_{\mathrm{PAULI}} = 0.268$ eV). The splitting of the two states starts at the excitonic coupling stage, with the excitation energy of one state lowered by 0.035 eV, and the other raised by 0.035 eV. When polarization and charge transfer are incorporated subsequently, the excitation energies of both states red-shift, while the splitting is still present.

In the Ne_2^* case, as each monomer has three degenerate excitations, $2p_x \rightarrow 3s$, $2p_y \rightarrow 3s$ and $2p_z \rightarrow 3s$, six fragment states are taken into account. In the supersystem, the two $2p_z \rightarrow 3s$ excitations are inequivalent to $2p_x \rightarrow 3s$ and $2p_y \rightarrow 3s$ (the z axis is along the vector between Ne atoms), thus their frozen states are slightly higher in energy than the other four. The six states further split when they are allowed to mix. The lowest and highest excitonic states (of A_{1g} and A_{1u} symmetries, respectively) are the in-phase and out-of-phase

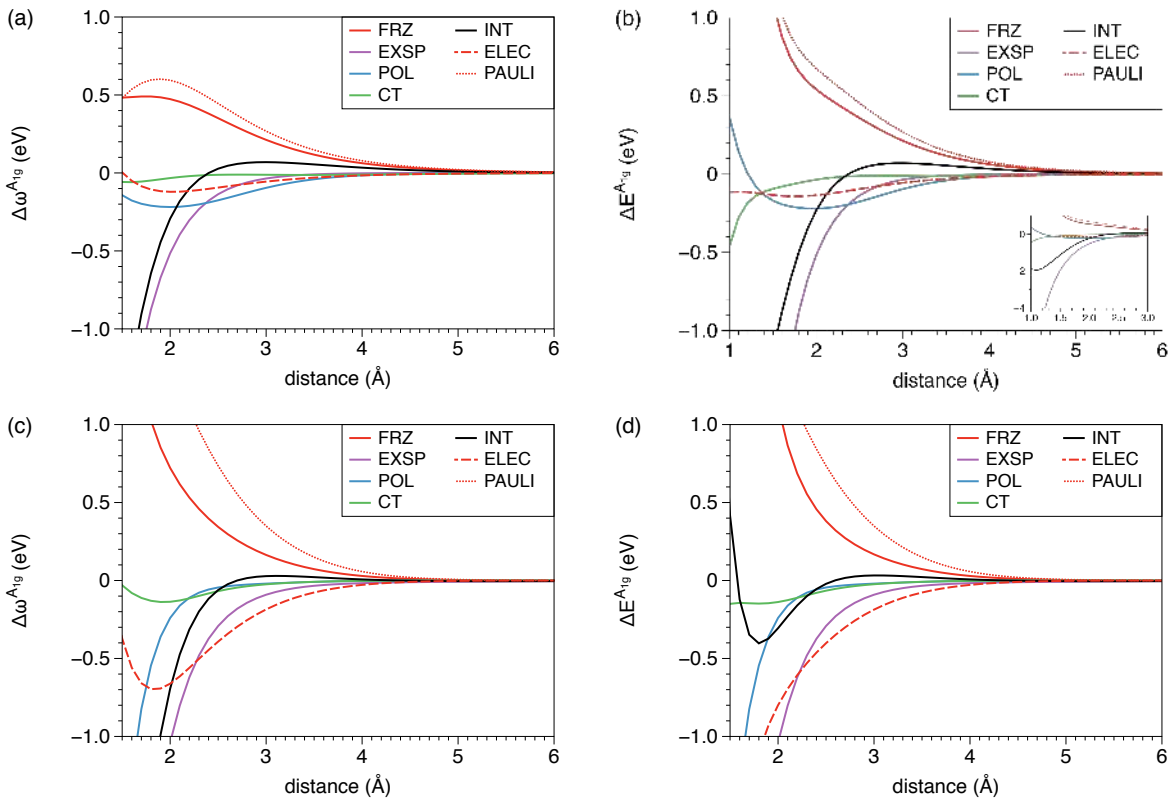

Figure 2: EDA results for the lowest singlet excited state (2^1A_{1g}) of He_2^* and Ne_2^* computed at different interatomic distances. (a) Decomposition of the excitation energy of He_2^* relative to the $1s \rightarrow 2s$ excitation energy of an isolated He atom. (b) Decomposition of the excited state interaction energy of He_2^* relative to separated He^* and He. (c) Same format as (a) but for Ne_2^* (d) Same format as (b) but for Ne_2^*.

combination of two fragment $2p_z \rightarrow 3s$ excitations, while the middle four states (two E_{1g} and two E_{1u}) come from $2p_x \rightarrow 3s$ and $2p_y \rightarrow 3s$ excitations. This can be confirmed by the linear combination coefficients solved from Eq. 12. Like the He_2^* case, all six states are stabilized by polarization and charge transfer.

Although the EDA terms are generally small at 3.0 Å for both He_2^* and Ne_2^*, the picture can be quite different at the equilibrium distances for the excited states. For He_2^*, the equilibrium is at 1.1 Å, with a well depth of 1.96 eV. For Ne_2^*, the equilibrium is at 1.8 Å, with a well depth of 0.40 eV. The energy levels (as in Fig. 1) evaluated at the excimer equilibrium distances can be found in the Supporting Information (Fig. S1), where the excitation energy splittings due to excitonic coupling are much larger. The effects of POL and CT also vary significantly: by contrast with Fig. 1, they do not always lower the excitation energies, and crossing of the higher-energy $2p_z \rightarrow 3s$ and $2p_{x(y)} \rightarrow 3s$ states occurs in Ne_2^* when CT is included.

Before moving on, we want to briefly discuss how to choose the fragment states. In particular, how many local excitations should be taken as the basis in Eq. 12? Let us consider what happens if the six $1s \rightarrow 2p$ excitations are also included for He_2^*. Solving the 8×8 generalized eigenvalue problem instead, we find that the results are different from those of the 2×2 case. $\omega^{1,2}_{\mathrm{EXSP}}$ values are now quite close to $\omega^{1,2}_{\mathrm{POL}}$, that is, $\Delta\omega^{1,2}_{\mathrm{POL}} \approx 0$ ($\omega^{1}_{\mathrm{EXSP}} = 21.221$ eV, $\omega^{2}_{\mathrm{EXSP}} = 21.263$ eV, $\omega^{1}_{\mathrm{POL}} = 21.220$ eV, $\omega^{2}_{\mathrm{POL}} = 21.264$ eV). A careful examination of the eigenvectors can explain the origin of this change. The first two excitonic states contain contributions from both $1s \rightarrow 2s$ and $1s \rightarrow 2p_z$ excitations, as $|\Psi_1^{1s\rightarrow 2s}\rangle \pm |\Psi_2^{1s\rightarrow 2s}\rangle$ are of the same symmetry as $|\Psi_1^{1s\rightarrow 2p_z}\rangle \pm |\Psi_2^{1s\rightarrow 2p_z}\rangle$ (both are A_{1g}) and they can mix further with each other, which is effectively a relaxation of fragment amplitudes. In other words, a considerable amount of polarization is contained in $\Delta\omega^{1,2}_{\mathrm{EXSP}}$, rendering $\Delta\omega^{1,2}_{\mathrm{POL}}$ tiny. Therefore the best choice of the degenerate subspace from the viewpoint of isolating the excitonic splitting is the minimal space of two strictly degenerate states, rather than the expanded 8-dimensional

space, which is at most quasi-degenerate. It may be interesting to using the present EDA to re-analyze the nature of states in larger helium clusters, where a band of $2s$-derived states and another band of $2p$-derived states are found.[62,63,67]

For Ne_2^*, although the EDA is performed on the six states all together, excitations of different symmetries (e.g. $2p_x \rightarrow 3s$ and $2p_z \rightarrow 3s$) are not allowed to mix. In fact, the 6×6 matrices in Eq. 12 are block-diagonal and each eigenvector has only two nonzero elements, corresponding to the excitation from the same $2p$ orbital of each Ne atom. This means that the EDA results are the same if we treat $2p_x \rightarrow 3s$, $2p_y \rightarrow 3s$ and $2p_z \rightarrow 3s$ separately.

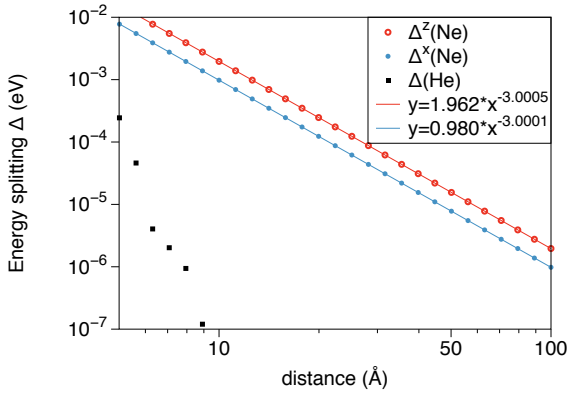

Figure 3: Log-log plot of excitonic splitting, Δ, in the lowest singlet excited states of He_2 and Ne_2 at large interatomic distances ($R > 5$ Å). Δ is calculated as $\Delta = |\Delta\omega^-_{\mathrm{EXSP}}| + |\Delta\omega^+_{\mathrm{EXSP}}|$, where $\Delta\omega^-_{\mathrm{EXSP}}$ and $\Delta\omega^+_{\mathrm{EXSP}}$ are the excitonic coupling terms for the out-of-phase and in-phase states, respectively. Excitonic splitting in He_2^* (labeled as Δ; shown as black dots) exhibits rapid decay with R, while it exhibits R^{-3} polynomial decay in Ne_2^*, consistent with Eq. 17. For Ne_2^*, Δ^z (red dots) refers to the $2p_z \rightarrow 3s$ splitting, while Δ^x (blue dots) refers to the $2p_x \rightarrow 3s$ splitting.

We then investigate the distance dependence of EDA terms for the 2^1A_{1g} state of He_2^*, and the 2^1A_{1g} state of Ne_2^*. The results are shown in Fig. 2. These two states are the lowest dimer states of their respective systems at all distances we studied. It is clear that in the binding regime, the most favorable term is the excitonic splitting. The large value of $\Delta\omega_{\mathrm{EXSP}}$ leads to the formation of excimers while the ground states are repulsive. For both He_2^* and Ne_2^*, polarization and charge transfer have minimal effects on energies, especially at larger

distances. This is consistent with the value of the overlaps, $\langle\Phi_{\mathrm{EXSP}}|\Phi_{\mathrm{POL}}\rangle$ and $\langle\Phi_{\mathrm{POL}}|\Phi_{\mathrm{FINAL}}\rangle$, which are very close to one. The long-range behavior of $\Delta\omega_{\mathrm{EXSP}}$, on the other hand, are different for He_2^* and Ne_2^*. Asymptotically, the energy splitting from excitonic coupling is proportional to the interaction between the two transition dipole moments of fragment excitations:

$$\Delta = \frac{2\mu_1\mu_2}{R^3}|(\cos(\theta_1 - \theta_2) - 3\cos\theta_1\cos\theta_2)| \tag{17}$$

where μ_1 and μ_2 are the magnitude of transition dipoles for non-interacting fragment 1 and 2, respectively. θ_1 and θ_2 are the angles between transition dipoles and the line connecting two fragments. For He_2^*, $\boldsymbol{\mu}(1s\rightarrow 2s) = \mathbf{0}$, and hence $\Delta\omega_{\mathrm{EXSP}}$ quickly decays to zero, although at short range it is the vital piece. As for Ne_2^*, monomer CIS calculations gives $\mu_1 = \mu_2 = 0.349$ a.u. Eq. 17 gives $\Delta^z = 1.959\ (\mathrm{eV}\cdot\mathrm{\AA}^3)R^{-3}$ for the splitting between the two states with $2p_z \rightarrow 3s$ parentage ($\theta_1 = \theta_2 = 0$). The splitting between the two states with $2p_{x/y} \rightarrow 3s$ parentage ($\theta_1 = \theta_2 = 90^\circ$) should be $\Delta^{x,y} = 0.979\ (\mathrm{eV}\cdot\mathrm{\AA}^3)R^{-3}$. We plot the calculated Δ^z and Δ^x against R for $R > 5$ Å in Fig. 3, which shows excellent agreement with the predicted relations. Meanwhile, the energy splitting of He_2^* is also shown in Fig. 3, and decays fast with distance.

3.2 2-pyridone dimer

The 2-pyridone (2-PY) dimer, a complex formed through cyclic, double N–H$\cdots$O=C hydrogen bonds, is analogous to nucleotide base pairs. The S1/S2 exciton splitting in the 2-PY dimer has been investigated both experimentally and theoretically.[68–72]

The ground state geometry of the 2-PY dimer (optimized at the ωB97X-D/6-311++G(d,p) level of theory[73]) is near-planar and has a C_{2h} symmetry (Fig. 4). The intermolecular center-of-mass distance R is found to be 5.25 Å.

With ωB97X-D/6-311++G(d,p), the first excitation energy of the monomer (using its

geometry in the dimer) is found to be 4.738 eV. The lowest two excited states of the dimer system, whose excitation energies are 4.805 eV and 4.957 eV, respectively, correspond to the out-of-phase and in-phase coupling of the first monomer excitation:

$$S_1 : \Phi^{A_g} = \Psi_1\Psi_2^* - \Psi_1^*\Psi_2$$

$$S_2 : \Phi^{B_u} = \Psi_1\Psi_2^* + \Psi_1^*\Psi_2$$

Note that S_1 and S_2 states have A_g and B_u symmetry, respectively. The calculated energy splitting (0.152 eV) is in fairly good agreement with the CC2 result (0.136 eV) by Sagvolden and coworkers,[72] who found that density functionals with large fractions of exact exchange are necessary to reproduce the CC2 splittings. The influence of the percentage of exact exchange was further investigated by Neugebauer *et al.* using subsystem TDDFT calculations based on coupled frozen density embedding,[74,75] which revealed that the effect of exact exchange is mainly on monomer transition densities.[76]

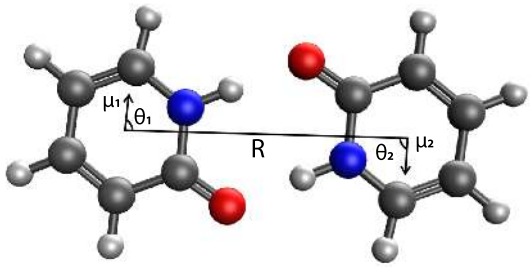

Figure 4: The structure of the ground state 2-PY dimer optimized with ωB97X-D/6-311++G(d,p).

The EDA results are shown in Table 1. The two hydrogen bonds in the ground state give binding energy of around 1 eV, with roughly 40% of the stabilization originating from CT, which is consistent with other hydrogen-bonded systems described by the ALMO-EDA.[77]

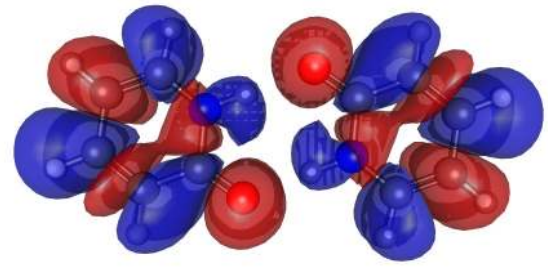

(a) S1

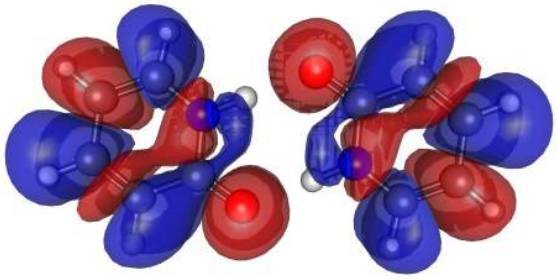

(b) S2

Figure 5: Difference density ($\Delta\rho = \rho^* - \rho$) plots for the lowest two excited states for the 2-PY dimer. The contour planes are placed at 0.0002 a.u.$^{-3}$, with positive ones in blue and negative ones in red.

Despite the excitonic splitting, the excimer EDA reveals that the complex is slightly destabilized in both S_1 and S_2 states compared to the ground state, mostly as a result of the less favorable electrostatics. This may be related to the weakening of hydrogen bonds. The difference densities $\Delta\rho = \rho^* - \rho$ of the excited states support this assumption, as the electronic densities are depleted on oxygen atoms and increased on hydrogen atoms upon excitation (see Fig. 5).

The degeneracy of the monomer excitations breaks once the two states delocalize. The splitting due to excitonic coupling is $\Delta = 2 \times 0.062$ eV $= 0.124$ eV, while the full calculation gives $\Delta = (0.222 - 0.070)$ eV $= 0.152$ eV, suggesting that the splitting caused by polarization and charge transfer (in this case, mainly CT) cannot be overlooked. We can also estimate the splitting based purely on the interaction between monomer transition dipoles, i.e, using Eq. 17. Based on our electronic structure calculation, $\mu_1 = \mu_2 = 1.161$ a.u., $\theta_1 = \theta_2 = 88.3°$, which gives $\Delta = 0.075$ eV at $R = 5.252$ Å. This is an underestimation compared to the

exciton model, most likely because the exchange effect is absent in the dipole-dipole model. Our results qualitatively agree with the CC2/aug-cc-pVTZ results reported by Leutwyler *et al.*,[69] in which a full *ab initio* calculation of vertical excitation energies predicted $\Delta = 1125$ cm^{-1}(0.139 eV), and the dipole-dipole model gave $\Delta = 745$ cm^{-1}(0.092 eV).

Table 1: EDA results of the 2-PY dimer (in eV), including the decomposition of interaction energies in the ground state and the first two excited states, as well as the shifts in excitation energies.

	FRZ	(ELEC/PAULI)	EXSP	POL	CT	INT
ΔE	-0.228	-1.610/1.381	-	-0.378	-0.437	-1.043
ΔE^{A_g}	-0.076	-1.483/1.406	-0.062	-0.381	-0.454	-0.973
$\Delta\omega^{A_g}$	0.152	0.127/0.025	-0.062	-0.004	-0.017	0.070
ΔE^{B_u}	-0.076	-1.483/1.406	0.062	-0.383	-0.424	-0.821
$\Delta\omega^{B_u}$	0.152	0.127/0.025	0.062	-0.005	0.013	0.222

Finally, it is noteworthy that experimentally, as the out-of-phase transition is dipole-forbidden, one has to break the symmetry, typically by introducing isotopes, to observe the energy splitting. Leutwyler and coworkers measured the fluorescence emission of 2-PY dimer and found a splitting of 43.5 cm^{-1}(0.0053 eV,[68] which is ~ 25 times smaller than the *ab initio* value. They showed that by multiplying the pure electronic splitting with a quenching factor, $\Gamma = \exp(-\sum_i S_i)$, where S_i is the Huang-Rhys factor of the i-th vibrational coordinate, the experimental result can be nicely reproduced.[71]

We also report the EDA results for the S_1 and S_2 states at their separately optimized geometries in the Supporting Information (Table S2). For S_1 and S_2, the intermolecular center-of-mass distances are 5.28 Å and 5.32 Å, respectively. The results, in general, are very similar to those reported in Table 1. It is noteworthy that the EXSP terms at the S_1 and S_2 minima are of slightly larger magnitude than that calculated at the ground state minimum, despite the smaller intermolecular separation in the latter. This might be associated with

variations of the monomer geometries in these optimized complex structures.

3.3 Benzene excimer

The smallest aromatic excimer is the benzene excimer. In its ground state, the parallel displaced configuration is most stable, while the sandwich configuration (with D_{6h} symmetry) is preferred in the excited state. At large distances, the lowest four states are the exciton resonance states, which originate from the two singlet excitation on each monomer (B_{2u}, B_{1u}):

$$\Phi^{B_{1g}} = \Psi_1^{A_{1g}}\Psi_2^{B_{2u}} - \Psi_1^{B_{2u}}\Psi_2^{A_{1g}}$$
$$\Phi^{B_{2u}} = \Psi_1^{A_{1g}}\Psi_2^{B_{2u}} + \Psi_1^{B_{2u}}\Psi_2^{A_{1g}}$$
$$\Phi^{B_{2g}} = \Psi_1^{A_{1g}}\Psi_2^{B_{1u}} - \Psi_1^{B_{1u}}\Psi_2^{A_{1g}}$$
$$\Phi^{B_{1u}} = \Psi_1^{A_{1g}}\Psi_2^{B_{1u}} + \Psi_1^{B_{1u}}\Psi_2^{A_{1g}}$$

We performed EDA calculations on the D_{6h} dimers at varying intermolecular distances ranging from 2.6 Å to 6.0 Å. The monomer geometry is optimized with the ωB97X-D functional[73] and 6-311++G(d,p) basis[78] and remains unchanged in the scan of intermolecular separation. The EDA is performed at the TD-ωB97X-D/6-311++G(d,p) level of theory.

With the values of $\langle\Phi_{\mathrm{EXSP}}|\Phi_{\mathrm{POL}}\rangle$ and $\langle\Phi_{\mathrm{POL}}|\Phi_{\mathrm{FINAL}}\rangle$ in hand, we are able to track the four states listed above. The magnitude of the overlaps between excitonic states and polarized states are very close to 1 (> 0.97 for all distances and all four states), which implies minimal polarization. On the other hand, the overlaps between polarized states and final states are considerably smaller, especially when the two benzene molecules are close to each other. The smallest magnitude of POL-FINAL overlap is ~ 0.74. This is still adequate to indicate a one-to-one connection between the final state (i.e. including charge transfer effects) and the polarized states.

The EDA results for the B_{1g} state are shown in Fig. 6. The excitonic splitting effect is rather small, which is not surprising as the corresponding monomer state has zero transition dipole moment. Meanwhile, CT plays the most essential role. The large magnitude of $\Delta\omega_{\mathrm{CT}}$ at binding region suggests that the stabilization effect of CT is much stronger in the excited state than in the ground state. The EDA results reveal a different mechanism for the formation of benzene excimer than the noble gas excimers, where the latter are mainly stabilized by the excitonic splitting effect. It was proposed that the formation of aromatic excimers is due to configuration mixing between ER states and CR states of the same symmetry. In 1965, Azumi and McGlynn[79] identified low-lying CR states of benzene dimer with B_{1g}, B_{2u}, B_{2g} and B_{1u} symmetries that can mix with the corresponding ER states. This is consistent with our results, as in the EDA procedure, the energy lowering due to CT mostly comes from removal of the constraint on excitation amplitudes (only intrafragment amplitudes can be nonzero), that is, allowing the charge-transfer type of configurations to be mixed into the wavefunctions.

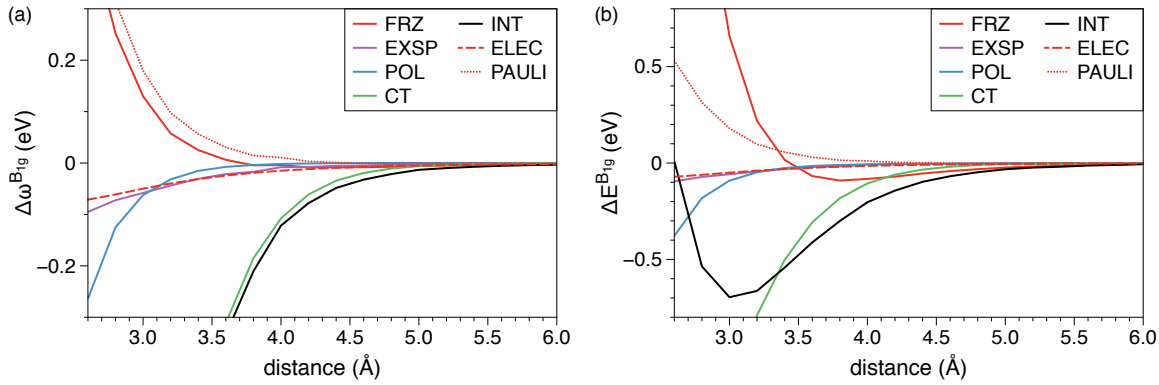

Figure 6: EDA results for the benzene dimer at different intermolecular distances. Decomposition of (a) the shifts in excitation energies and (b) excited state interaction energies for the B_{1g} state are presented.

We also obtain the potential energy curves of the ground state (A_{1g}) and four ER states with B_{1g}, B_{2u}, B_{2g} and B_{1u} symmetries (Fig. 7(c)). Significant binding is found for the B_{1g} and B_{2g} states, which are more favored by CT than the other two excited states. A crossing

between B_{2u} and B_{2g} is observed at $\sim$ 3.3 Å. This crossing has been predicted by other authors, but at a different distance ($\sim$ 2.8 Å).[80] Asymptotically, the energies of all states approach the corresponding monomer state limit. Potential energy curves are also plotted for other intermediate wavefunctions(Fig. 7(a),(b)). The polarized PESs show no strong binding for all states, and no state-crossing either, which again emphasizes the importance of CT. The excitonic curves deviate only slightly from the frozen curves (indicated by dashed lines in Fig. 7(a)), as both parent monomer states are dipole-forbidden.

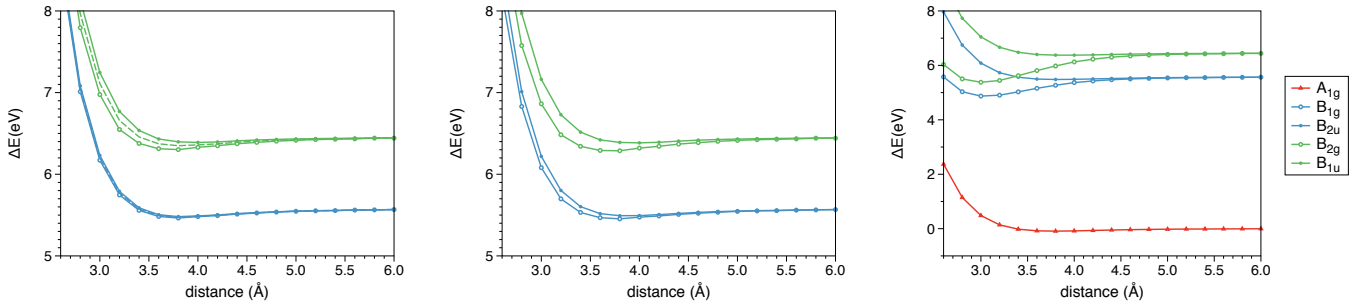

(a) EXSP/FRZ (b) POL (c) FINAL

Figure 7: The potential energy surfaces for the ground state (A_{1g}) and four excited states (B_{1g}, B_{2u}, B_{2g} and B_{1u}) of the benzene dimer (of D_{6h} symmetry). The energies are referenced to the energy of the ground-state monomers at infinite separation. The distance between two benzene rings is varied from 2.6 Å to 6.0 Å. (a): The energies after excitonic coupling (solid line) and frozen energies (dashed line); (b): The energies after polarization; (c): The energies of final wavefunctions (with CT included).

.

3.4 Perylene excimer

Now we turn to another aromatic excimer, the perylene excimer. EDA calculations are performed on the sandwich dimer with D_{2h} symmetry (Fig. 8). The monomer geometry optimization employs the ωB97X-D functional and 6-31+G(d) basis, and the EDA is performed at the TD-ωB97X-D/6-31+G(d) level of theory. We investigated the two states that

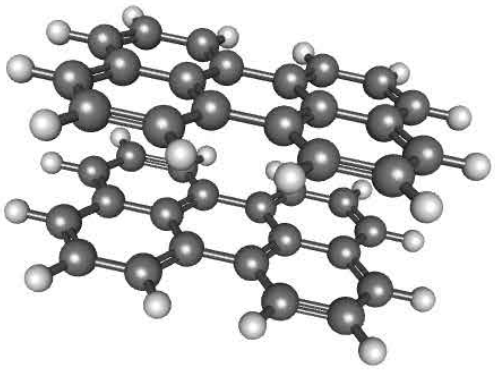

Figure 8: Structure of the D_{2h} perylene dimer constructed from monomer geometries optimized with ωB97X-D/6-31+G(d).

come from the lowest monomer state (B_{2u}):

$$\begin{aligned}\Phi^{B_{3g}} &= \Psi_1^{A_{1g}}\Psi_2^{B_{2u}} - \Psi_1^{B_{2u}}\Psi_2^{A_{1g}} \\ \Phi^{B_{2u}} &= \Psi_1^{A_{1g}}\Psi_2^{B_{2u}} + \Psi_1^{B_{2u}}\Psi_2^{A_{1g}}\end{aligned} \tag{18}$$

Like the benzene dimer, the magnitude of overlaps imply small polarization and relatively large charge transfer, yet the EDA results (shown in Fig. 9) still reveal some unique features in the perylene case.

In contrast to benzene's $\Phi^{B_{1g}}$ states, the $\Phi^{B_{3g}}$ of perylene corresponds to a monomer state with large transition dipole moment (2.728 a.u.), thus we expect a strong stabilization effect from the exciton coupling. This is verified by the EDA results, shown in Fig. 9. Charge transfer is strongly favorable as well. However, the distance dependence of charge transfer and excitonic splitting are quite different. Close to the equilibrium distance ($\sim$ 3.4 Å), CT is dominant, and for this reason we regard it as the most crucial factor in the formation of perylene excimer. At larger distances, CT rapidly diminishes as it is believed to be correlated

with the overlap between two fragments, which decays exponentially. The excitonic splitting term, as we discussed before, has an R^{-3} asymptotic behavior, allowing it to eventually surpass CT and become the most important term. Our EDA predicts this turnover at ~ 4.2 Å, where the curves corresponding to $\Delta\omega^{B_{3g}}_{\mathrm{EXSP}}$ and $\Delta\omega^{B_{3g}}_{\mathrm{CT}}$ cross.

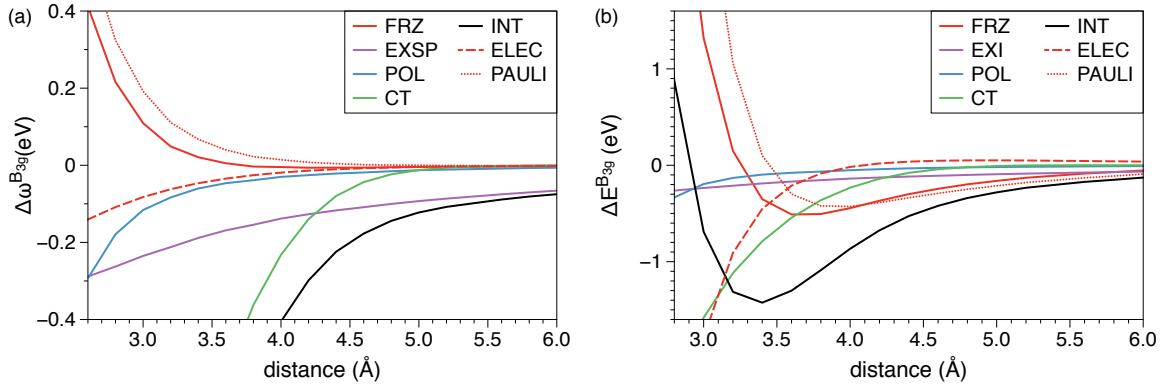

Figure 9: EDA results for the perylene dimer at different intermolecular distances. Decomposition of (a) the shift in excitation energies and (b) excited state interaction energies for the B_{3g} state are presented.

The potential energy surfaces for the ground state (A_{1g}) and two excited states (B_{3g}, B_{2u}) of the D_{2h} perylene dimer are shown in Fig. 10. The B_{3g} state has a binding energy that is notably larger than that of the ground state, owing to its more favorable CT. Meanwhile, the weaker binding of B_{2u} state is more likely due to dispersion rather than CT as it is already present at the frozen stage. Recalling that in the benzene dimer, the B_{2u} and B_{1u} states are not much favored by CT either, we wonder if it is a general trend that CT is stronger in the out-of-phase states than in the in-phase states. We also note that all binding energies are ~ 0.9 eV stronger than those computed by Kuhlman and coworkers previously,[81] who utilized BH&HLYP/6-31G(d)[82] level of theory. We attribute this discrepancy to the dispersion interaction, which is not accounted for by BH&HLYP. A comparison of EDA results using BH&HLYP and ωB97X-D is shown in Table S3 of the Supporting Information. At 3.6 Å, the major difference comes from the Pauli term of the ground state (about 1 eV more favorable with ωB97X-D), which, under the current scheme, incorporates all non-

electrostatic effects at the frozen level, including dispersion.

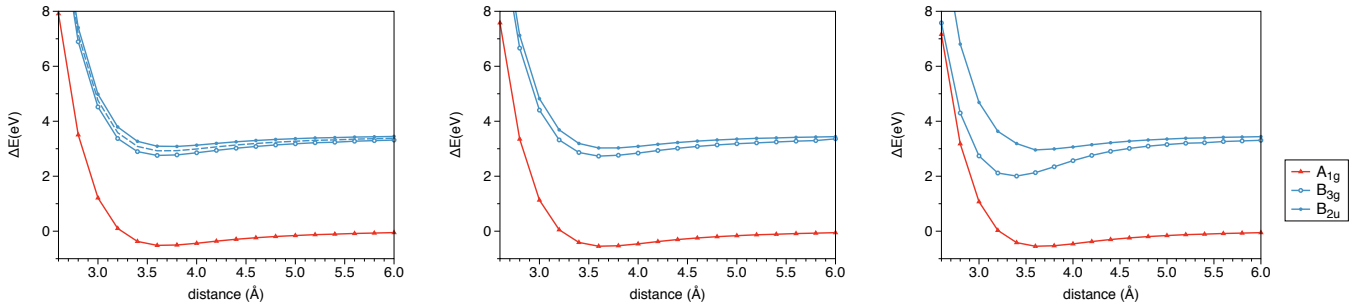

(a) EXSP/FRZ (b) POL (c) FINAL

Figure 10: The potential energy surfaces for the ground state (A_{1g}) and two excited states (B_{3g}, B_{2u}) of the D_{2h} perylene dimer. The energies are referenced to the energy of the ground-state monomers at infinite separation. The distance between two benzene rings is varied from 2.6 Å to 6.0 Å. (a): The energies after excitonic coupling (solid line) and frozen energies (dashed line); (b): The energies after polarization; (c): The energies of the final states (with CT included).

4 Conclusion

In the present paper, we have generalized the previously proposed ALMO-EDA scheme[52] for intermolecular interactions involving excited molecules in exciplexes to include the excitonic coupling that can be important for describing excimers. The EDA is based on linear response theory (e.g. CIS, TDDFT), and it connects degenerate initial (reference) states of monomers to the final supersystem states of an excited complex.

The energy difference between the final and initial states defines the interaction energy, which is decomposed into frozen (FRZ), excitonic splitting (EXSP), polarization (POL) and charge-transfer (CT) terms. The partition is achieved by evaluating the energy of three intermediate states subject to different constraints, i.e., the frozen, excitonic splitting and polarized states.

At the frozen level, both MOs and amplitudes are unrelaxed (taking their values from isolated fragment calculations), and each excited fragment state corresponds to one frozen

state, constructed by embedding the fragment state into the environment of other ground state fragments. The exciton-splitting states are the new intermediate states introduced in this paper to describe the excitonic coupling effect in excimers. They are linear combinations of the frozen states, obtained by solving the secular equation in the basis of the frozen states. The ALMO-CIS wavefunctions[62] are utilized as the polarized states. In ALMO-CIS, intra-fragment relaxation of MOs and amplitudes is allowed and the excited states of the supersystem are constructed as superposition of intrafragment excitations.

From another point of view, more configurations are allowed to contribute to each supersystem wavefunction when the constraints are gradually removed: the excitonic states allow mixing between nearly degenerate local excitations on different fragments, the polarized states allow mixing of all intrafragment excitations, and the final states further incorporate all interfragment (CT-type) excitations.

While there is a one-to-one mapping between fragment states and frozen states, starting at the excitonic level, the mapping between states at different levels is non-trivial as the excitations become delocalized. We followed a "maximum overlap" scheme to track the states at each intermediate level, so that the new EDA scheme is able to treat multiple states in a reasonable way. Moreover, the overlap between intermediate states can often serve as a complementary validation for the EDA results.

With the generalization of the excited state EDA scheme, we are able to deal with situations where the excitation is delocalized across the whole system (e.g. excimers). We employed the EDA to study noble gas excimers including He_2^* and Ne_2^*, aromatic excimers including benzene and perylene excimer, as well as $(2\text{-pyridone})_2$, a hydrogen bonded system. We are able to reveal the dominant forces that contribute to the formation of these excimers. For example, the excitonic splitting effect is important for noble gas excimers, while CT is significant in aromatic excimers. The EDA terms are also shown to have correct asymptotic behavior.

Although this work focused on excimer systems, the current EDA scheme is fully compatible with localized excitations (e.g. exciplexes), which was the main subject of our initial report.[52] In exciplexes, typically one fragment has an excited state whose excitation energy is significantly lower than possible excitations on other fragments, so this state only weakly couples with other fragment states because of the large energy gap. This will result in an EXSP term that is zero by definition, and the improved EDA scheme then reduces to its previous form.

Finally, we note that the current method still retains some limitations of the previous EDA scheme for exciplexes: (i) lack of an explicit separation of dispersion effects (they are lumped as part of the FRZ term); (ii) lack of a useful basis set limit for the POL and CT terms. The latter shortcoming has been discussed in the context of ground state EDA,[83–86] and the fragment electric response function (FERF) approach[84] was proposed to address this issue. Using a given truncated multipole order for the FERFs, the convergence of POL (and thus CT) with respect to the size of the employed basis set can be restored. It is an interesting open question as to whether such the FERF approach can be usefully extended or generalized to excited states.

While the method presented here is already of practical use, the limitations mentioned above, as well as the quest for an EDA based on higher-level theories for excited states, raise non-trivial challenges for future work. Furthermore, we have always been taking local excitations as reference states and considering the EDA terms in a sequence that goes from (typically) longest to shortest range. Such a sequence is certainly not unique, and it may be interesting to develop an EDA scheme starting from charge-transfer states for cases where they are of greater importance.

Associated Content

Supporting Information

Estimation of the magnitude of BSSE for excimers at the equilibrium distances of their lowest excited states; additional EDA results for He_2^* and Ne_2^* at equilibrium interatomic distances, for the 2-pyridone dimer at the optimal structures of the S1 and S2 states, and for the perylene dimer at 3.6 Å using BH&HLYP and ωB97X-D functionals.

Acknowledgments

This work was supported by the Director, Office of Science, Office of Basic Energy Sciences, of the U.S. Department of Energy under Contract No. DE-AC02-05CH11231. The authors thank Dr. Yuezhi Mao for useful discussions and comments on the manuscript.

References

(1) Birks, J.; Munro, I. *Prog. React. Kinet.* **1967**, *4*, 239.

(2) Hopfield, J. J. *Astrophys. J* **1930**, *72*, 133.

(3) Cheshnovsky, O.; Raz, B.; Jortner, J. *Chem. Phys. Lett.* **1972**, *15*, 475–479.

(4) Freeman, C.; McEwan, M.; Claridge, R.; Phillips, L. *Chem. Phys. Lett.* **1971**, *10*, 530–532.

(5) Oka, T.; Rao, K. R.; Redpath, J.; Firestone, R. *J. Chem. Phys.* **1974**, *61*, 4740–4746.

(6) Förster, T.; Kasper, K. *Berichte der Bunsengesellschaft für physikalische Chemie* **1955**, *59*, 976–980.

(7) Conlon, P.; Yang, C. J.; Wu, Y.; Chen, Y.; Martinez, K.; Kim, Y.; Stevens, N.; Marti, A. A.; Jockusch, S.; Turro, N. J.; Tan, W. *J. Am. Chem. Soc.* **2008**, *130*, 336–342.

(8) Dembo, M.; Glushko, V.; Aberlin, M. E.; Sonenberg, M. *Biochimica et Biophysica Acta (BBA)-Biomembranes* **1979**, *552*, 201–211.

(9) Nagatoishi, S.; Nojima, T.; Juskowiak, B.; Takenaka, S. *Angew. Chem.* **2005**, *117*, 5195–5198.

(10) Focsaneanu, K.-S.; Scaiano, J. *Photochem. Photobiol. Sci* **2005**, *4*, 817–821.

(11) Schoenfisch, M. H.; Zhang, H.; Frost, M. C.; Meyerhoff, M. E. *Anal. Chem.* **2002**, *74*, 5937–5941.

(12) Frenkel, J. *Phys. Rev.* **1931**, *37*, 17.

(13) Davydov, A. *Theory of molecular excitons*; Springer, 2013.

(14) Krueger, B. P.; Scholes, G. D.; Fleming, G. R. *J. Phys. Chem. B* **1998**, *102*, 5378–5386.

(15) Morrison, A. F.; You, Z.-Q.; Herbert, J. M. *J. Chem. Theory Comput.* **2014**, *10*, 5366–5376.

(16) Li, X.; Parrish, R. M.; Liu, F.; Kokkila Schumacher, S. I.; Martínez, T. J. *J. Chem. Theory Comput.* **2017**, *13*, 3493–3504.

(17) Hoffmann, M.; Schmidt, K.; Fritz, T.; Hasche, T.; Agranovich, V.; Leo, K. *Chem. Phys.* **2000**, *258*, 73–96.

(18) Phipps, M. J. S.; Fox, T.; Tautermann, C. S.; Skylaris, C.-K. *Chem. Soc. Rev.* **2015**, *44*, 3177–3211.

(19) Pastorczak, E.; Corminboeuf, C. *J. Chem. Phys.* **2017**, *146*, 120901.

(20) Rybak, S.; Jeziorski, B.; Szalewicz, K. *J. Chem. Phys.* **1991**, *95*, 6576–6601.

(21) Jeziorski, B.; Moszynski, R.; Szalewicz, K. *Chem. Rev.* **1994**, *94*, 1887–1930.

(22) Żuchowski, P. S.; Podeszwa, R.; Moszyński, R.; Jeziorski, B.; Szalewicz, K. *J. Chem. Phys.* **2008**, *129*, 084101.

(23) Szalewicz, K. *Wiley Interdiscip. Rev.: Comput. Mol. Sci.* **2012**, *2*, 254–272.

(24) Hohenstein, E. G.; Sherrill, C. D. *Wiley Interdiscip. Rev.: Comput. Mol. Sci.* **2012**, *2*, 304–326.

(25) Kitaura, K.; Morokuma, K. *Int. J. Quantum Chem.* **1976**, *10*, 325–340.

(26) Morokuma, K. *Acc. Chem. Res.* **1977**, *10*, 294–300.

(27) Ziegler, T.; Rauk, A. *Theor. Chem. Acc.* **1977**, *46*, 1–10.

(28) Ziegler, T.; Rauk, A. *Inorg Chem* **1979**, *18*, 1558–1565.

(29) von Hopffgarten, M.; Frenking, G. *Wiley Interdiscip. Rev.: Comput. Mol. Sci.* **2012**, *2*, 43–62.

(30) Bagus, P. S.; Hermann, K.; Bauschlicher Jr, C. W. *J. Chem. Phys.* **1984**, *80*, 4378–4386.

(31) Stevens, W. J.; Fink, W. H. *Chem. Phys. Lett.* **1987**, *139*, 15–22.

(32) Su, P.; Li, H. *J. Chem. Phys.* **2009**, *131*, 014102.

(33) Su, P.; Jiang, Z.; Chen, Z.; Wu, W. *J. Phys. Chem. A* **2014**, *118*, 2531–2542.

(34) Mo, Y.; Gao, J.; Peyerimhoff, S. D. *J. Chem. Phys.* **2000**, *112*, 5530–5538.

(35) Mo, Y.; Song, L.; Lin, Y. *J. Phys. Chem. A* **2007**, *111*, 8291–8301.

(36) Khaliullin, R. Z.; Cobar, E. A.; Lochan, R. C.; Bell, A. T.; Head-Gordon, M. *J. Phys. Chem. A* **2007**, *111*, 8753–8765.

(37) Wu, Q.; Ayers, P. W.; Zhang, Y. *J. Chem. Phys.* **2009**, *131*, 164112.

(38) Mo, Y.; Bao, P.; Gao, J. *Phys. Chem. Chem. Phys.* **2011**, *13*, 6760–6775.

(39) Wu, Q. *J. Chem. Phys.* **2014**, *140*, 244109.

(40) Horn, P. R.; Sundstrom, E. J.; Baker, T. A.; Head-Gordon, M. *J. Chem. Phys.* **2013**, *138*, 134119.

(41) Thirman, J.; Head-Gordon, M. *J. Chem. Phys.* **2015**, *143*, 084124.

(42) Horn, P. R.; Mao, Y.; Head-Gordon, M. *Phys. Chem. Chem. Phys.* **2016**, *18*, 23067–23079.

(43) Mao, Y.; Horn, P. R.; Head-Gordon, M. *Phys. Chem. Chem. Phys.* **2017**, *19*, 5944–5958.

(44) Thirman, J.; Head-Gordon, M. *J. Phys. Chem. A* **2016**,

(45) Plasser, F.; Lischka, H. *J. Chem. Theory Comput.* **2012**, *8*, 2777–2789.

(46) Plasser, F.; Wormit, M.; Dreuw, A. *J. Chem. Phys.* **2014**, *141*, 024106.

(47) Plasser, F.; Bäppler, S. A.; Wormit, M.; Dreuw, A. *J. Chem. Phys.* **2014**, *141*, 024107.

(48) Plasser, F.; Thomitzni, B.; Bäppler, S. A.; Wenzel, J.; Rehn, D. R.; Wormit, M.; Dreuw, A. *J. Comput. Chem.* **2015**, *36*, 1609–1620.

(49) Spata, V. A.; Matsika, S. *J. Phys. Chem. A* **2014**, *118*, 12021–12030.

(50) Luzanov, A. V.; Casanova, D.; Feng, X.; Krylov, A. I. *J. Chem. Phys.* **2015**, *142*, 224104.

(51) Casanova, D.; Krylov, A. I. *J. Chem. Phys.* **2016**, *144*, 014102.

(52) Ge, Q.; Mao, Y.; Head-Gordon, M. *J. Chem. Phys.* **2018**, *148*, 064105.

(53) Dreuw, A.; Head-Gordon, M. *Chem. Rev.* **2005**, *105*, 4009–4037.

(54) Foresman, J. B.; Head-Gordon, M.; Pople, J. A.; Frisch, M. J. *J. Phys. Chem.* **1992**, *96*, 135–149.

(55) Marques, M. A.; Gross, E. K. U. *Annu. Rev. Phys. Chem.* **2004**, *55*, 427–455.

(56) Van Gisbergen, S.; Snijders, J.; Baerends, E. *Comput. Phys. Commun.* **1999**, *118*, 119–138.

(57) Casida, M. E. *J. Mol. Struc-Theochem* **2009**, *914*, 3–18.

(58) Hirata, S.; Head-Gordon, M. *Chem. Phys. Lett.* **1999**, *314*, 291–299.

(59) Stoll, H.; Wagenblast, G.; Preuß, H. *Theor. Chem. Acc.* **1980**, *57*, 169–178.

(60) Khaliullin, R. Z.; Head-Gordon, M.; Bell, A. T. *J. Chem. Phys.* **2006**, *124*, 204105.

(61) Boys, S. F.; Bernardi, F. d. *Molecular Physics* **1970**, *19*, 553–566.

(62) Closser, K. D.; Ge, Q.; Mao, Y.; Shao, Y.; Head-Gordon, M. *J. Chem. Theory Comput.* **2015**, *11*, 5791–5803.

(63) Ge, Q.; Mao, Y.; White, A. F.; Epifanovsky, E.; Closser, K. D.; Head-Gordon, M. *J. Chem. Phys.* **2017**, *146*, 044111.

(64) Horn, P. R.; Mao, Y.; Head-Gordon, M. *J. Chem. Phys.* **2016**, *144*, 114107.

(65) Mao, Y.; Demerdash, O.; Head-Gordon, M.; Head-Gordon, T. *J. Chem. Theory Comput.* **2016**, *12*, 54225437.

(66) Shao, Y.; Gan, Z.; Epifanovsky, E.; Gilbert, A. T.; Wormit, M.; Kussmann, J.; Lange, A. W.; Behn, A.; Deng, J.; Feng, X.; Ghosh, D.; Goldey, M.; Horn, P. R.; Jacobson, L. D.; Kaliman, I.; Khaliullin, R. Z.; Kuś, T.; Landau, A.; Liu, J.; Proynov, E. I.; Rhee, Y. M.; Richard, R. M.; Rohrdanz, M. A.; Steele, R. P.; Sundstrom, E. J.; Woodcock, H. L.; Zimmerman, P. M.; Zuev, D.; Albrecht, B.; Alguire, E.; Austin, B.; Beran, G. J. O.; Bernard, Y. A.; Berquist, E.; Brandhorst, K.; Bravaya, K. B.; Brown, S. T.; Casanova, D.; Chang, C.-M.; Chen, Y.; Chien, S. H.; Closser, K. D.; Crittenden, D. L.; Diedenhofen, M.; DiStasio, R. A.; Do, H.; Dutoi, A. D.; Edgar, R. G.; Fatehi, S.; Fusti-Molnar, L.; Ghysels, A.; Golubeva-Zadorozhnaya, A.; Gomes, J.; Hanson-Heine, M. W.; Harbach, P. H.; Hauser, A. W.; Hohenstein, E. G.; Holden, Z. C.; Jagau, T.-C.; Ji, H.; Kaduk, B.; Khistyaev, K.; Kim, J.; Kim, J.; King, R. A.; Klunzinger, P.; Kosenkov, D.; Kowalczyk, T.; Krauter, C. M.; Lao, K. U.; Laurent, A.; Lawler, K. V.; Levchenko, S. V.; Lin, C. Y.; Liu, F.; Livshits, E.; Lochan, R. C.; Luenser, A.; Manohar, P.; Manzer, S. F.; Mao, S.-P.; Mardirossian, N.; Marenich, A. V.; Maurer, S. A.; Mayhall, N. J.; Neuscamman, E.; Oana, C. M.; Olivares-Amaya, R.; ONeill, D. P.; Parkhill, J. A.; Perrine, T. M.; Peverati, R.; Prociuk, A.; Rehn, D. R.; Rosta, E.; Russ, N. J.; Sharada, S. M.; Sharma, S.; Small, D. W.; Sodt, A.; Stein, T.; Stück, D.; Su, Y.-C.; Thom, A. J.; Tsuchimochi, T.; Vanovschi, V.; Vogt, L.; Vydrov, O.; Wang, T.; Watson, M. A.; Wenzel, J.; White, A.; Williams, C. F.; Yang, J.; Yeganeh, S.; Yost, S. R.; You, Z.-Q.; Zhang, I. Y.; Zhang, X.; Zhao, Y.; Brooks, B. R.; Chan, G. K.; Chipman, D. M.; Cramer, C. J.; Goddard, W. A.; Gordon, M. S.; Hehre, W. J.; Klamt, A.; Schaefer, H. F.; Schmidt, M. W.; Sherrill, C. D.; Truhlar, D. G.; Warshel, A.; Xu, X.; Aspuru-Guzik, A.; Baer, R.; Bell, A. T.; Besley, N. A.; Chai, J.-D.; Dreuw, A.; Dunietz, B. D.; Furlani, T. R.; Gwaltney, S. R.; Hsu, C.-P.; Jung, Y.; Kong, J.; Lambrecht, D. S.; Liang, W.; Ochsenfeld, C.; Rassolov, V. A.; Slipchenko, L. V.; Subotnik, J. E.; Van Voorhis, T.; Herbert, J. M.; Krylov, A. I.;

Gill, P. M.; Head-Gordon, M. *Mol. Phys.* **2015**, *113*, 184–215.

(67) Closser, K. D.; Head-Gordon, M. *J. Phys. Chem. A* **2010**, *114*, 8023–8032.

(68) Müller, A.; Talbot, F.; Leutwyler, S. *J. Chem. Phys.* **2002**, *116*, 2836–2847.

(69) Ottiger, P.; Leutwyler, S.; Köppel, H. *J. Chem. Phys.* **2012**, *136*, 174308.

(70) Kopec, S.; Ottiger, P.; Leutwyler, S.; Köppel, H. *J. Chem. Phys.* **2012**, *137*, 184312.

(71) Ottiger, P.; Köppel, H.; Leutwyler, S. *Chem. Sci.* **2015**, *6*, 6059–6068.

(72) Sagvolden, E.; Furche, F.; Köhn, A. *J. Chem. Theory Comput.* **2009**, *5*, 873–880.

(73) Chai, J. D.; Head-Gordon, M. *Phys. Chem. Chem. Phys.* **2008**, *10*, 6615–6620.

(74) Casida, M. E.; Wesołowski, T. A. *Int. J. Quant. Chem.* **2004**, *96*, 577–588.

(75) Neugebauer, J. *J. Chem. Phys.* **2007**, *126*, 134116.

(76) König, C.; Neugebauer, J. *J. Phys. Chem. B* **2013**, *117*, 3480–3487.

(77) Khaliullin, R. Z.; Bell, A. T.; Head-Gordon, M. *Chem. Eur. J.* **2009**, *15*, 851855.

(78) Frisch, M. J.; Pople, J. A.; Binkley, J. S. *J. Chem. Phys.* **1984**, *80*, 3265–3269.

(79) Azumi, T.; McGlynn, S. *J. Chem. Phys.* **1965**, *42*, 1675–1680.

(80) Vala Jr, M. T.; Hillier, I. H.; Rice, S. A.; Jortner, J. *J. Chem. Phys.* **1966**, *44*, 23–35.

(81) Kuhlman, T. S.; Lemke, H. T.; Sølling, T. I.; Velardez, G. F.; Henriksen, N. E.; Møller, K. B. *J. Phys. Chem. A* **2009**, *113*, 6849–6850.

(82) Becke, A. D. *J. Chem. Phys.* **1993**, *98*, 1372–1377.

(83) Azar, R. J.; Horn, P. R.; Sundstrom, E. J.; Head-Gordon, M. *J. Chem. Phys.* **2013**, *138*, 084102.

(84) Horn, P. R.; Head-Gordon, M. *J. Chem. Phys.* **2015**, *143*, 114111.

(85) Lao, K. U.; Herbert, J. M. *J. Chem. Theory Comput.* **2016**, *12*, 2569–2582.

(86) Mao, Y.; Ge, Q.; Horn, P. R.; Head-Gordon, M. *J. Chem. Theory Comput.* **2018**, *14*, 2401–2417.

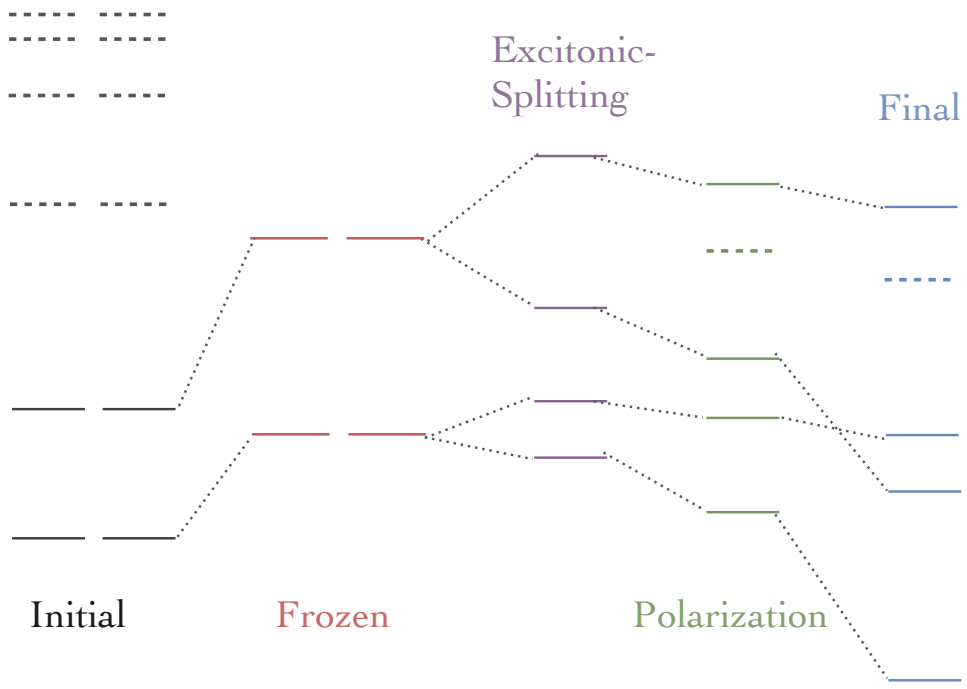

Figure 11: For Table of Contents (TOC) only